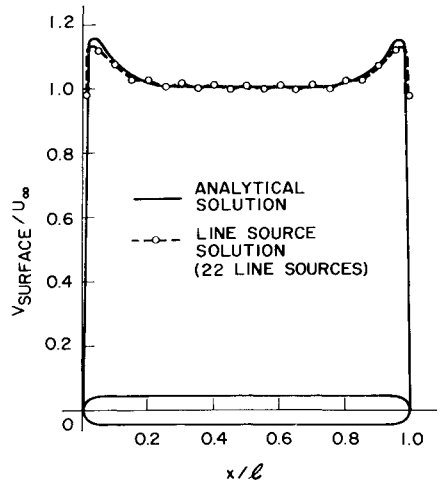

Fig. 2 Comparison of analytical and line source solutions for a Rankine oval of fineness ratio 10.

to the line sources causes an increased local effect of the line sources which, as a result, gives rise to the surface rippling. The rippling was more pronounced using 20 sources as compared to 40 sources because the surface was less restricted with the smaller number of sources. The surface velocity using 20 sources was still within 1% of analytical values, so the solution was considered adequate.

An attempt was made to duplicate the velocity distribution about a body given by Smith and Pierce.[4] The shape was a smooth body of revolution with a large annular bump near the nose (Fig. 3). Smith and Pierce state that the method of axial line sources predicts an incorrect velocity distribution over the body. A more accurate statement, however, of their conclusion is that the zero streamline for a system of line sources cannot follow the contour of the body, and therefore, cannot be used to calculate the velocities around it. The results for line sources given by Smith and Pierce were obtained by reducing the number of body coordinates until the zero streamline could pass thrugh all of them, but these were too few to accurately describe the body. This example showed that the method of axial line sources cannot generate a body with relatively large deviations in surface slope.

Another class of bodies that were generated by von Kármán's method was cones. The results for the potential flow around cones were generally good when the included angle of the cone was less than a certain value. The only part of the cone that was not accurately generated, as would be expected, was the cone tip. The tip of the generated cone was slightly rounded because the lead line source was positive. It was found from numerical experiments that for a given number of sources there is a maximum included angle the cone may have before the method breaks down. For 20 sources, the maximum included angle was found to be 51.8°. If it is attempted to generate a cone with this included angle with 40 sources, the solution will again break down. It is evident, therefore, that the method of axial line source is not only sensitive to the contour of the body, but also the number of sources used to generate it.

IV. Conclusions

Von Kármán's method of axial line sources produces a linear system of simultaneous equations which, in general, is ill-conditioned. Very high accuracy is, therefore, required in calculating the equations and finding their solution. Our results indicate that the method of axial line sources is not generally practical on digital computers that have less than 20_{10} or 25_{10} significant figure accuracy.

Von Kármán's method does not always produce reliable solutions for the potential flow around a specified body. To determine if the solution is accurate, at least two checks must be made; first, check if the zero streamline passes through all the specified coordinates of the body, and second, check if the velocity is well behaved along the body surface.

To determine if von Kármán's method is applicable for a certain body, it is not sufficient to state simply that the body need only be slender and lacking discontinuities in surface slope. The present investigation concludes that there are several interrelated factors, some of which were documented here, that determine if an accurate solution can be obtained.

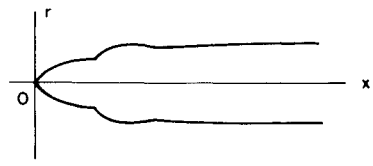

Fig. 3 Body of revolution with large annular bump as given by Ref. 4.

References

[1] Von Kármán, T., "Berechnung der Druckverteilung an Luftschiffkörpern," *Abhandlungen aus dem Aerodynamischen Institut an der Technischen Hochschule Aachen*, No. 6, 1927, pp. 3–17; also TN574, July 1930, NACA.

[2] Karamcheti, K., *Principles of Ideal-Fluid Aerodynamics*, Wiley, New York, 1966, pp. 343–344.

[3] Watson, L. E., "Incompressible Potential Flow Solutions for Bodies of Revolution by the Method of Axial Line Sources," MS thesis, Aug. 1971, University of Texas at Austin, Austin, Texas.

[4] Smith, A. M. O. and Pierce, J., "Exact Solution of the Neumann Problem. Calculation of Noncirculatory Plane and Axially Symmetric Flows about or within Arbitrary Boundaries," Douglas Rept. ES 26988, April 1958, McDonald-Douglas Aircraft Co., St. Louis, Mo.

Shock Shapes of Blunt Bodies in Hypersonic Helium, Air, and CO_2 Flows

CHARLES G. MILLER* AND JOHN A. MOORE*
NASA Langley Research Center, Hampton, Va.

Nomenclature

M_∞ = freestream Mach number
$N_{Re,\infty}$ = freestream unit Reynolds number, m^{-1}
p_t = stagnation point pressure, kN/m^2
p_∞ = freestream static pressure, kN/m^2
r_b = model base radius, m
r_n = spherical nose radius, m
T_t = stagnation point temperature, °K
T_∞ = freestream temperature, °K
U_∞ = freestream velocity, km/sec
x, r = cylindrical coordinates (see Fig. 2)
γ = ratio of specific heats
γ_{eff} = effective ratio of specific heats
$\gamma_{E,2}$ = postnormal shock static isentropic exponent
$\gamma_{E,\infty}$ = freestream isentropic exponent
Δ = ratio of shock standoff distance to model base radius
ε = normal-shock density ratio
ρ_∞ = freestream density, gm/m^3
θ = cone semiapex angle, deg

Introduction

A PRIMARY factor governing hypersonic flowfield characteristics of blunt vehicles entering planetary atmospheres is

Received October 5, 1973.
Index categories: Supersonic and Hypersonic Flow; Shock Waves and Detonations.

* Aero-Space Engineer, Hypervelocity Impulse Facilities Section, Space Systems Division.

Table 1 Calculated freestream and postnormal shock flow conditions

Gas	p_∞	ρ_∞	T_∞	$\gamma_{E,\infty}$	M_∞	$N_{Re,\infty} \times 10^{-5}$	U_∞	ε	γ_{eff}	$\gamma_{E,2}$	p_t	T_t
He	1.31	2.02	305	1.67	6.82	6.63	7.04	3.76	1.67	1.67	88.9	5077
Air	2.14	6.97	1068	1.33	8.45	8.62	5.40	11.35	1.16	1.15	196.5	6273
CO_2	1.17	4.74	1308	1.17	9.29	5.09	5.00	18.86	1.09	1.15	116.5	3858

the normal shock density ratio. Hence, a means of duplicating or simulating the high density ratios experienced during planetary entry is needed. One facility having the capability of generating a range of hypersonic-hypervelocity flow conditions in arbitrary test gases is the expansion tube. The purpose of this Note is to present preliminary shock shape results obtained in the Langley 6-in. expansion tube at hypersonic conditions. Normal shock density ratios from approximately 4 to 19 were generated using helium, air, and CO_2 test gases at freestream velocities from 5 to 7 km/sec. Test models were a flat-faced cylinder and the Viking aeroshell.

Apparatus and Tests

A brief description of the Langley 6-in. diam expansion tube is presented in Ref. 1. For the present tests, the driver gas was unheated helium at a nominal pressure of 33 MN/m^2. Test gases were helium, air, and CO_2, and the initial test gas pressure was 3.45 kN/m^2 for all three gases. For a given test, the acceleration gas was the same as the test gas, but at a much lower quiescent pressure.[1] Vertical pitot pressure surveys with a 9-probe rake showed the test core flow to be uniform and have a diameter of approximately half the tube diameter for all conditions of this study.

Models tested were a flat-faced cylinder and the Viking aeroshell, a spherically blunted cone having $\theta = 70°$ and $r_n/r_b = 0.5$. The r_b for the flat-faced cylinder and the aeroshell was 2.86 cm and 2.54 cm, respectively. The results presented herein are for zero angle of attack.

Shock shapes were obtained with a single-pass schlieren system. The point light source, which had a duration of approximately 150 nsec, was pulsed during the quasi-steady test flow period. These shapes were recorded on 10.16×12.70 cm negatives and read manually from enlargements to twice model size for the aeroshell and to model size for the flat-faced cylinder. A photograph illustrating the shock shape on the aeroshell model for CO_2 test gas is presented in Fig. 1. Readings from these enlargements are believed to be accurate to within 0.13 mm. The shock resolution on enlargements for helium tests was less than that for air and CO_2, due to the lower flow density and index of refraction for helium. Hence, a greater uncertainty in reading the shock displacement exists for the helium tests, with this uncertainty increasing with vertical distance from the stagnation point. The Δ was also inferred from densitometer scans of the negatives; these Δ agreed to within 6% of those obtained by manual reading for all tests. The maximum uncertainty in measured shock displacement is believed to be less than $\pm 10\%$.

Freestream and postnormal shock flow conditions were calculated using the thermochemical equilibrium program of Ref. 2. Measured inputs to this program were 1) acceleration gas-test gas interface velocity (U_∞), 2) tube wall pressure (p_∞), and 3) stagnation point pressure (p_t). Nominal values of measured inputs were used to calculate the following flow conditions for each test gas. The value p_t represents an average value across the test core as obtained with the 9-probe survey rake. (Units for flow quantities are given in nomenclature.)

Results and Discussion

Shock shapes for the flat-faced cylinder model are shown in Fig. 2 for the three test gases. For the conditions of this study, the inviscid forebody flow should be relatively insensitive to M_∞ and primarily dependent on ε (Mach number independence principle, Ref. 3). The Reynolds number, based on conditions behind the normal portion of the shock and on body diameter, is greater than 10^4 for all test gases. Hence, Δ should be independent of Reynolds number.[4] (At sufficiently low Reynolds numbers, the shock and boundary-layer thicknesses are no longer negligible compared to shock detachment distance. In this regime, Δ increases with decreasing Reynolds number.) Also shown in Fig. 2 are shock shapes calculated using the one-strip integral method of Ref. 5. This method is restricted to an ideal

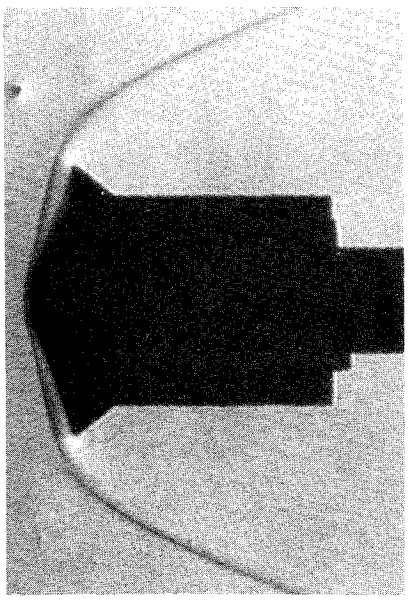

Fig. 1 Photograph of shock shape on Viking aeroshell for CO_2 test gas.

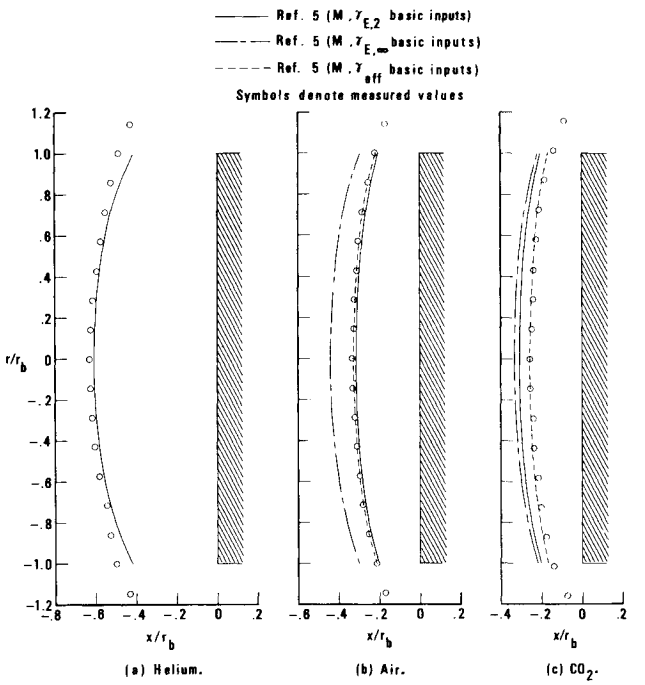

Fig. 2 Shock shapes for flat-faced cylinder.

gas (constant γ) and to blunt bodies with sonic corners. The basic inputs to the method of Ref. 5 are M_∞, γ and model geometry. The broken lines of Fig. 2 represent shock shapes calculated for M_∞ and $\gamma_{E,\infty}$ as basic inputs; the solid lines denote M_∞ and $\gamma_{E,2}$ as basic inputs; the dashed lines denote M_∞ and γ_{eff} as basic inputs. The γ_{eff} was determined from the ideal-gas, normal shock relation

$$\gamma_{\text{eff}} = [1+\varepsilon(1-2/M_\infty{}^2)]/(\varepsilon-1)$$

where M_∞ and ε are real-gas, equilibrium values obtained from Ref. 2.

The expected decrease in measured shock detachment distance with increasing ε is illustrated in Fig. 2, with Δ decreasing by a factor of 2.5 as ε increases from 4 to 19. Relatively good agreement exists between measured and calculated shock shapes for helium as expected, since the present helium flow conditions correspond to ideal-gas behavior ($\gamma_{E,\infty} = \gamma_{E,2} = \gamma_{\text{eff}}$). For air and CO_2, the agreement between measured and calculated shock shape improves when $\gamma_{E,2}$, instead of $\gamma_{E,\infty}$, is used as an input to the program of Ref. 5. When γ_{eff} is used as input, the measured and calculated shock shapes are observed to be in good agreement. This result supports the proposal (for example, Ref. 6) that flowfield calculations for blunt bodies where real-gas effects are significant can be greatly simplified by use of ideal-gas relations with an appropriate γ.

In Fig. 3, measured and calculated shock shapes for the Viking aeroshell model are presented for the three test gases. This figure, in conjunction with Fig. 2, illustrates the effect of body shape on shock shape and detachment distance. The effect of body shape becomes more pronounced as ε increases. For example, the ratio of measured Δ for the flat-faced cylinder to measured Δ for the aeroshell is approximately 1.9 for helium ($\varepsilon = 3.8$), 4 for air ($\varepsilon = 11.4$), and 7 for CO_2 ($\varepsilon = 18.9$). Again, the measured and calculated results for helium are observed to be in good agreement, and usage of γ_{eff} in the program of Ref. 5 improves agreement between measured and calculated shock shapes; however, this agreement for the Viking aeroshell is somewhat poorer than that for the flat-faced cylinder.

A problem characteristic of high-enthalpy facilities, such as the expansion tube, is determination of the thermochemical state of the flow. Results obtained in the Langley pilot model expansion tube with oxygen-nitrogen mixtures showed departure of the freestream flow from equilibrium (Ref. 7). Although nonequilibrium freestream effects on Δ should be small for air, freestream departure from equilibrium for CO_2 may be shown to decrease ε, thus increase standoff distance. For both test gases, nonequilibrium flow in the shock layer of the model will have an appreciable effect on Δ, with Δ for nonequilibrium flow being greater than that for equilibrium flow.[8] Additional studies are required to determine the possible extent of nonequilibrium in the postshock flow. However, the present tests suggest that for standoff distances of the order of those observed on the flat-faced cylinder model, nonequilibrium effects are relatively small; for the much smaller standoff distance of the Viking aeroshell model, some postshock nonequilibrium effects may be evident for CO_2. It should be noted, however, that a change in γ_{eff} for CO_2 of only 1.6% is required to bring the calculated shock displacement into agreement with measured shock displacement. Overall, the present results have verified that shock shapes observed in the hypersonic, real-gas flow of the expansion tube over a wide range of ε may be accurately described by simple, ideal-gas calculations (Ref. 5) provided γ_{eff} is used as input.

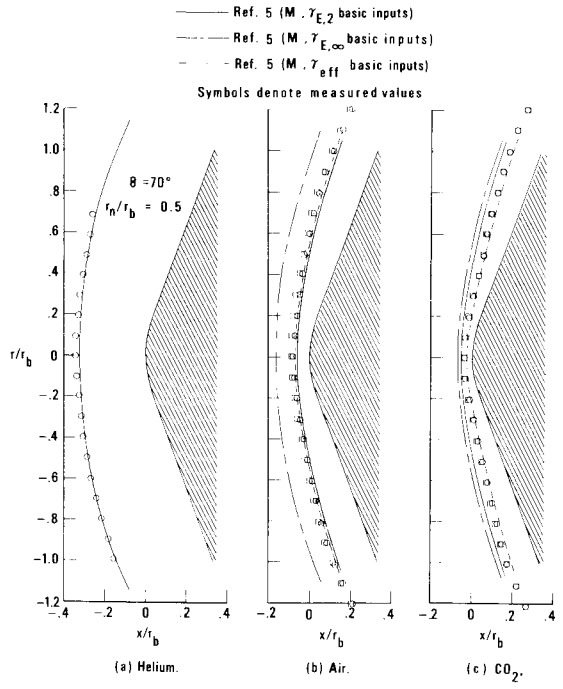

Fig. 3 Shock shapes for Viking aeroshell.

References

[1] Miller, C. G., III, "A Program for Calculating Expansion-Tube Flow Quantities for Real-Gas Mixtures and Comparison With Experimental Results," TN D-6830, 1972, NASA.

[2] Miller, C. G., III, "Computer Program of Data Reduction Procedures for Facilities Using CO_2–N_2–O_2–Ar Equilibrium Real-Gas Mixtures," TM X-2512, 1972, NASA.

[3] Hayes, W. D. and Probstein, R. F., *Hypersonic Flow Theory*, Academic Press, New York, 1966,

[4] Bailey, A. B. and Sims, W. H., "Shock Detachment Distance for Blunt Bodies in Argon at Low Reynolds Number," *AIAA Journal*, Vol. 1, No. 12, Dec. 1963, pp. 2867–2868.

[5] South, J. C., Jr., "Calculation of Axisymmetric Supersonic Flow Past Blunt Bodies with Sonic Corners, Including a Program Description and Listing," TN D-4563, 1968, NASA.

[6] Lomax, H. and Inouye, M., "Numerical Analysis of Flow Properties About Blunt Bodies Moving at Supersonic Speeds in an Equilibrium Gas," TR R-204, 1964, NASA.

[7] Haggard, K. V., "Free-Stream Temperature, Density, and Pressure Measurements in an Expansion Tube Flow," TN D-7273, 1973, NASA.

[8] Kuehn, D. M., "Experimental and Theoretical Pressures on Blunt Cylinders for Equilibrium and Nonequilibrium Air at Hypersonic Speeds," TN D-1979, 1963, NASA.

Lift and Moment for Arbitrary Power-Law Upwash in Oscillating Subsonic Unsteady Thin-Airfoil Theory

NELSON H. KEMP*
Avco Everett Research Lab. Inc., Everett, Mass.

Introduction

IN oscillating unsteady airfoil theory, various types of chordwise upwash distributions are of interest, depending on the application. Classical flutter studies made use of constant and linear upwash distributions, which are appropriate to plunging and pitching airfoils. Sears[1] introduced the sinusoidal gust, and Kemp[2] introduced the generalized sinusoidal gust in which the time and space frequencies are different.

For incompressible flow, the lift and moment expressions for these upwashes are well known. The constant and linear results are in books on Aeroelesticity while the sinusoidal gust results

Received October 23, 1973.
Index category: Nonsteady aerodynamics.
* Principal Research Scientist.